Journal of Nuclear Materials 399 (2010) 68–80

Contents lists available at ScienceDirect

Journal of Nuclear Materials

journal homepage: www.elsevier.com/locate/jnucmat

Oxidizing dissolution of spent MOX47 fuel subjected to water radiolysis: Solution chemistry and surface characterization by Raman spectroscopy

C. Jégou [a,*], R. Caraballo [a], J. De Bonfils [a], V. Broudic [a], S. Peuget [a], T. Vercouter [b], D. Roudil [a]

[a] Commissariat à l'Énergie Atomique (CEA), Marcoule Reasearch Center, B.P. 17171, F-30207 Bagnols-sur-Cèze Cedex, France
[b] Commissariat à l'Énergie Atomique (CEA), Saclay Reasearch Center, B.P. 11, F-91191 Gif-sur-Yvette Cedex, France

ARTICLE INFO

Article history:
Received 3 September 2009
Accepted 5 January 2010

Keywords:
MOX fuel
Actinides
Leaching
Radiolysis
Raman spectroscopy

ABSTRACT

The mechanisms of oxidizing dissolution of spent MOX fuel (MIMAS TU2®) subjected to water radiolysis were investigated experimentally by leaching spent MOX47 fuel samples in pure water at 25 °C under different oxidizing conditions (with and without external gamma irradiation); the leached surfaces were characterized by Raman spectroscopy. The highly oxidizing conditions resulting from external gamma irradiation significantly increased the concentration of plutonium (Pu(V)) and uranium (U(VI)) compared with a benchmark experiment (without external irradiation). The oxidation behavior of the plutonium-enriched aggregates differed significantly from that of the UO_2 matrix after several months of leaching in water under gamma irradiation. The plutonium in the aggregates appears to limit fuel oxidation. The only secondary phases formed and identified to date by Raman spectroscopy are uranium peroxides that generally precipitate on the surface of the UO_2 grains. Concerning the behavior of plutonium, solution analysis results appear to be compatible with a conventional explanation based on an equilibrium with a $Pu(OH)_{4(am)}$ phase. The fission product release – considered as a general indicator of matrix alteration – from MOX47 fuel also increases under external gamma irradiation and a change in the leaching mode is observed. Diffusive leaching was clearly identified, coinciding with the rapid onset of steady-state actinide concentrations in the bulk solution.

1. Introduction

In the eventuality of interim wet storage of MOX fuel assemblies for several decades the prospect of a through-wall cladding defect must be taken into consideration. In the event of a failed fuel element the main objective is to determine the potential impact of the formation of secondary phases or an oxidized layer on the cladding behavior. The irradiation conditions expected in a fuel storage pool (high γ dose rate in the fuel assembly and contact with aerated water) will be favorable to the recombination kinetics in favor of the molecular species like hydrogen peroxide liable to enhance oxidizing dissolution of the fuel matrix near the defect. Over the long-term, precipitation and/or oxidation phenomena will potentially have two contradictory effects: one liable enlarge the opening around the cladding defect as a result of volume expansion due to mechanical stresses related to the formation of secondary phases, and the other tending to diminish the fuel leach rate by filling the pellet gap and cracks. Extended tests lasting 5 to 10 years on UOX fuel segments (UOX fuel, 30 to 60 GWd t_{HM}^{-1}) have always demonstrated a drop in the long-term fuel alteration rate together with filling of voids by the precipitation of secondary phases [1–3], i.e. water penetration into a fuel rod appears to be limited by crack filling phenomena. For spent MOX fuel little information is available concerning oxidation under radiolysis or the nature of the phases and/or oxidized layers likely to form. The microstructural and chemical heterogeneity of MOX fuel with highly variable plutonium concentrations generally complicates the interpretation of the results.

We therefore investigated the radiolytic oxidation mechanisms of MOX47 spent fuel under conditions representative of underwater interim storage and the formation of secondary phases by combining solution analysis with Raman spectroscopy, which can now be implemented in a hot cell to analyze highly irradiating materials. The optimum conditions for obtaining suitable Raman spectra – i.e. representative of the surface condition of spent MOX47 fuel after radiolytic oxidation – have already been determined on model materials [4]. The sensitivity of the material samples to temperature and laser power required a large number of tests but allowed us to identify the secondary phases present on Pu-doped UO_2 samples after leaching, and to obtain benchmark spectra for UO_2 and PuO_2 [4]. This preliminary work was followed by the initial

* Corresponding author. Address: Commissariat à l'Énergie Atomique (CEA), Marcoule Center, DTCD/SECM/LMPA, BP 17171, F-30207 Bagnols-sur-Cèze Cedex, France. Tel.: +33 466 791642; fax: +33 466 797708.
E-mail address: christophe.jegou@cea.fr (C. Jégou).

0022-3115/$ - see front matter © 2010 Elsevier B.V. All rights reserved.
doi:10.1016/j.jnucmat.2010.01.004

characterization of spent MOX47 fuel and spectroscopic examination after extended leaching in water under gamma irradiation in aerated conditions.

2. Experimental

2.1. Spent fuel characteristics and leaching history

The spent fuel, designated MOX47 in the remainder of this article, was a MIMAS MOX TU2® fuel sample with an initial Pu/(Pu + U) enrichment of 6.6 wt.% irradiated in the Dampierre2 reactor for four cycles from 15 November 1993 to 16 May 1998. The mean burnup in the rod from which the samples were taken was 48.8 GWd t_{HM}^{-1}.

Prior to irradiation the microstructure observed on this type of MOX fuel [5] revealed the presence of three zones arising from the fabrication process (dilution of a UO_2 and PuO_2 oxide blend in UO_2 powder) and from the origin of the UO_2 powder:

- a phase with low Pu content (about 2.7%) but containing 15% of the total plutonium, referred to in the remainder of this document as the UO_2 matrix;
- a phase of aggregates with high Pu content (about 20%) comprising 38% of the total plutonium, known as the plutonium-rich aggregates;
- a phase of intermediate Pu content (about 7%) encapsulating the two preceding phases and accounting for 47% of the total Pu.

Under the sintering conditions (oxygen potential $\Delta G_{O_2} \approx -420$ kJ mol^{-1}) and for standard plutonium concentrations, the U—Pu—O phase diagram shows that the $(U_{1-y}Pu_y)O_2$ solid solution forms over a wide range that extends with the temperature [6,7]. For kinetic reasons, however, the solid solution is not fully formed and the MOX microstructure exhibits irregularities.

After irradiation the mean plutonium content is about 3.6 wt.%. There are still plutonium-rich aggregates that were restructured in the reactor with a local burnup some 2.5 times higher than the mean value. Some aggregates contain as much as 15 to 18% plutonium, and most about 10%. Well over half the plutonium is found in the intermediate encapsulation phase, and the remainder in equal amounts in the UO_2 matrix and in the aggregates. The mass fractions and mean thermal power were calculated using the Cesar code [8] as of the date of the MOX47 fuel leaching experiments (Table 1). Despite the material heterogeneity the mean values will be used to interpret the leaching results. Inventory calculations for different burnup levels (up to 150 GWd t_{HM}^{-1}) showed that the local concentrations of the various classes of fission products (especially cesium and strontium) are proportional to the burnup. The heterogeneity of the local burnup therefore does not discount the methodology developed for UOX fuel. The Cs/Sr congruence ratios near 1 for the fractions released into solution should continue to provide data on MOX fuel matrix alteration in general, whether the UO_2 matrix, the intermediate zone, or the Pu-rich aggregates. It is clear, however, that the heterogeneity of the actinide chemical composition between the aggregates, the intermediate zone, and the matrix will affect the oxidation behavior in each zone. Moreover, redox potential gradients can also be expected on the fuel surface between Pu-rich aggregates and the UO_2 matrix.

Two groups of 4 and 5 fragments were used to carry out two separate leaching experiments. The actual masses of the test fragments and their leaching history are indicated in Fig. 1. All the fragments were sampled from the core of a single clad segment and were previously leached for several months in carbonated water (10^{-3} M Na_2CO_3) to eliminate as much as possible of the Cs and Sr inventories in the cracks, in the open porosity, and at the grain boundaries. As the objective was to investigate fuel matrix alteration, it was very important to eliminate the radionuclide inventories outside the $(U_{1-y}\ Pu_y)O_2$ grains and aggregates in order to use cesium and strontium as $(U_{1-y}\ Pu_y)O_2$ matrix alteration tracers.

Table 1
Mass fractions of the major isotopes and elements analyzed in solution to monitor spent MOX47 fuel matrix alteration and thermal power levels.

Isotope/element	x_i MOX47
U	8.01E−01
Pu	3.56E−02
^{236}Pu	1.23E−10
^{237}Pu	7.75E−24
^{238}Pu	1.39E−03
^{239}Pu	1.30E−02
^{240}Pu	1.22E−02
^{241}Pu	5.61E−03
^{242}Pu	5.35E−03
^{243}Pu	6.75E−18
^{244}Pu	5.17E−07
^{241}Am	3.19E−03
^{244}Cm	5.74E−04
Cs	1.27E−03
^{134}Cs	8.19E−06
^{137}Cs	1.26E−03
Sr	4.72E−04
^{90}Sr	2.60E−04
^{86}Sr	1.97E−07
^{88}Sr	2.11E−04
^{89}Sr	4.00E−24
Thermal power	W t_{HM}^{-1} (MOX47)
α	3.5E+03
β	1.3E+03
γ	1.0E+03

A clad segment of spent MOX47 fuel was also characterized by Raman spectroscopy before and after extended leaching.

2.2. Leaching protocols

2.2.1. Leach tests on spent fuel fragments

Two leaching experiments on MOX47 spent fuel fragments with a burnup of 48.8 GWd t_{HM}^{-1} are compared in this study (Fig. 1) to assess fuel matrix alteration when subjected to water radiolysis under different oxidizing conditions.

Before each experiment the spent fuel fragments were subjected to at least five preleaching cycles under aerated conditions. Each one-hour preleaching cycle was performed in 10 mL of deionized or carbonated water (10^{-3} M Na_2CO_3). The purpose of the preleaching was also to avoid a U(VI) release peak due to surface oxidation that could skew the estimated total quantity of uranium oxidized during the leaching experiments. The cycles were repeated until steady-state conditions were obtained, corresponding to a reference state. The following experiments were carried out:

- *Experiment 1*: Benchmark experiment in pure aerated water without external gamma irradiation.
- *Experiment 2*: In aerated pure water in the presence of an external gamma irradiation source (^{60}Co) generating a dose rate of 320 Gy h^{-1} to reproduce as closely as possible the radiation field inside a fuel assembly.

From the standpoint of water radiolysis and the magnitude of oxidizing conditions, significant differences can be expected between the two experiments. Prior radiolysis calculations for similar experiments on UOX60 fuel [9,10] revealed highly oxidizing conditions for experiment 2 in the bulk solution in contact with the source; moreover, the concentration gradients of oxidizing agents were reversed between the two configurations.

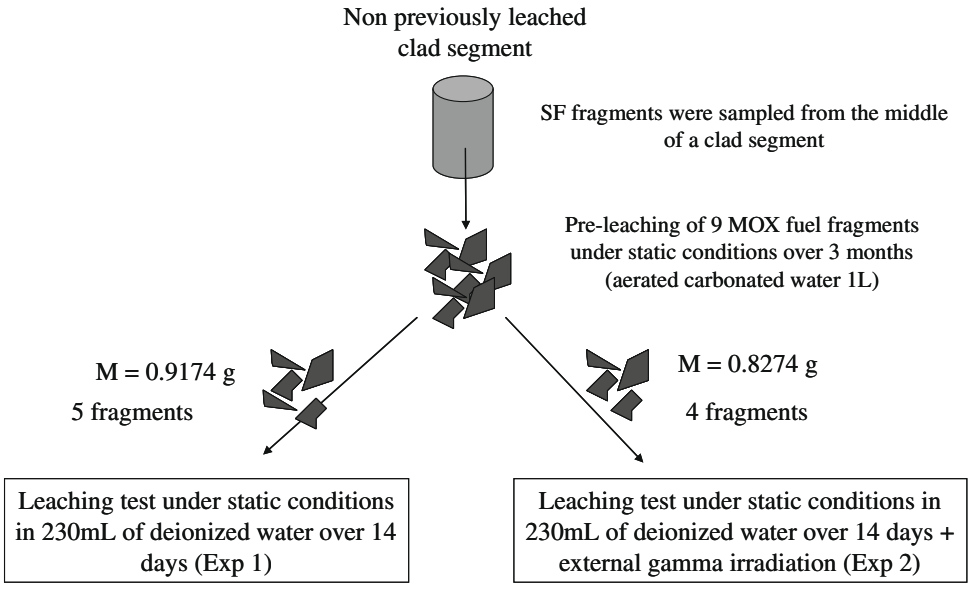

Fig. 1. Summary of leaching experiments performed on spent MOX47 fuel fragments.

For experiment 1, considering the small quantities of fuel involved, irradiation was mainly local and involved α radiation (with a range of 40 μm in water) and β radiation (400 μm in water). The concentration profile of oxidizing, radical and molecular species at the interface was therefore similar to the result obtained by Lundström or Poulesquen [11,12], i.e. with a peak near the spent fuel due to the consumption of species on the surface, and significantly decreasing away from the irradiated zone due to diffusion of species into the unirradiated homogeneous solution, which constitutes a "sink".

For experiment 2, the presence of a source produced oxidizing species in the homogeneous solution; the diffusion of radicals and molecular species generated by radiolysis from the spent fuel/water reaction interface into the homogeneous solution was thus limited. In other words, the source maintained the oxidizing species generated by the fuel at the solid–liquid interface. The consumption of oxidizing species on the spent fuel surface ultimately leads to a gradient from the homogeneous solution toward the interface [13].

These gradients directly affect redox potentials, actinide release into the homogeneous solution and solubility [9,10].

Leaching experiments lasting 14 days were carried out in a hot cell in deionized water (initial pH = 6.2) under static conditions (without solution renewal, V = 230 mL) at room temperature (25 °C). Static leaching conditions were selected to enhance oxidation and secondary phase precipitation on the fuel surface while avoiding any removal of material by large-scale diffusion processes or by flowing solution.

Solution samples were taken after 1 h, and after 1, 3, 7, 10 and 14 days for elemental and radiochemical analysis. A few additional samples were also filtered (0.45 μm) and ultrafiltered (10,000 Da) to estimate the colloid fraction.

After each experiment the spent MOX fuel fragments were removed from the sample holder and dried in air. After measuring the leachate pH, nitric acid (14 N HNO_3) was added to acidify the leachate in the leaching vessel to 0.5 N and restore the initial volume of 230 mL. The sample holder was also immersed in the acidified solution to recover the activity bound to the components of the leaching device in order to obtain a comprehensive assessment. After one day of acidification, a sample was taken and the solution was discarded. The vessel was rinsed one last time for 24 h with 230 mL of 0.5 N HNO_3 to solubilize any remaining precipitates or colloids that could have been deposited on the vessel walls or on the sampling tube.

For the MOX47 fuel leaching experiments the redox potential of the bulk solution was measured using an Ag/AgCl electrode (KCl 3 mol L^{-1}) with a platinum probe. The electrode voltage with respect to the hydrogen electrode was +207 mV at 25 °C.

2.2.2. Leach tests on spent fuel segment

A clad MOX47 fuel segment was leached for 3 months in pure aerated water under external gamma irradiation (320 Gy h^{-1}); the surfaces of the plutonium-rich aggregates and UO_2 matrix were analyzed by Raman spectroscopy at intervals of 0, 1, 7, and 18 days, 1 month and 3 months.

Prior to leaching the sample was polished to a mirror finish on one face. Selective chemical etching of the UO_2 grains was performed on the polished face to separate the UO_2 grains from the $(U_{1-y}\ Pu_y)O_2$ aggregates. The etching solution was a mixture of 40 cm^3 of H_2SO_4 (commercial 110-vol solution, 30 wt.%) and 45 cm^3 of H_2O_2 (2 M). The etching solution was poured into a Petri dish containing several thicknesses of Kimtex® wipers on which the sample was absorbed. Etching was repeated several times for a total sample/solution contact time of 105 s; between each attack the sample material was rinsed with distilled water and observed under an optical microscope. This initial characterization was essential in that it separated the plutonium-enriched aggregates from the UO_2 matrix on the outer surface and facilitated the identification of the zones for the acquisition of Raman spectra during the extended leaching experiment.

During the leaching experiment the segment was removed from the leaching vessel for Raman spectrometry, then returned to the irradiator until the next sampling interval.

2.2.3. Solution analysis

The uranium in solution was assayed using a kinetic phosphorescence analyzer (KPA) capable of determining uranium over a concentration range from 0.5 to 100 μg L^{-1}, i.e. 2×10^{-9} to 4×10^{-7} mol L^{-1}. Higher concentrations (mg L^{-1}) were analyzed by ICP-AES or by KPA after dilution. The plutonium isotopes were analyzed by alpha spectrometry.

Gamma spectrometry was used to determine the cesium concentrations (^{134}Cs and ^{137}Cs) in the leachates and β counting was used to determine the ^{90}Sr concentrations.

Hydrogen peroxide, a stable product generated by water radiolysis, was analyzed in the bulk solution by spectrophotometry (Ghormley method) for concentrations ranging from 4×10^{-6} to 2×10^{-4} mol L^{-1} and by chemiluminescence for lower concentrations ranging from 1×10^{-9} to 6×10^{-7} mol L^{-1}.

2.2.4. Solution analysis results

The analysis results are expressed as concentrations or as fractions of the total inventory released into solution. It is unnecessary to include and estimate a surface area parameter because the spent fuel fragments have the same history and the same morphology, and can therefore be compared according to the alteration conditions [10]. Any estimate of the reactive surface area is difficult due to structural reorganization of plutonium-rich aggregates and would introduce a further degree of uncertainty on the interpretation of the experimental results.

For a radionuclide X, the inventory fraction released in the aqueous phase (FIAP) is expressed as follows:

$$\mathrm{FIAP}_X = \frac{a_X^{\mathrm{sol}} V_{\mathrm{leachate}}}{A_X^{\mathrm{inv}} f_{\mathrm{U}} m_{(\mathrm{UPu})\mathrm{O}_2}} \quad (1)$$

where a_x^{sol} is the volume activity (Bq mL^{-1}) of radionuclide X in the aqueous phase in the leachate, A_x^{inv} the specific activity (Bq $g_{(\mathrm{U,Pu})}{}^{-1}$) of radionuclide X in the initial spent fuel inventory, V_{leachate} the leachate volume (mL), $m_{(\mathrm{UPu})\mathrm{O}_2}$ the initial oxide mass (g) in the spent fuel specimen, and f_U the uranium–plutonium metal mass conversion factor per gram of fuel.

In the case of a test under static conditions, p samples are taken from the leaching vessel; it is more relevant to follow the variation of the cumulative fraction of inventory in the aqueous phase for a radionuclide (or element) X at interval n ($1 \leqslant n \leqslant p$), i.e. $\sum \mathrm{FIAP}_X(n)$, which is directly related to the total release from the sample since the beginning of the experiment. This quantity is calculated as follows for any radionuclide X:

$$\mathrm{FIAP}c(n) = \sum \mathrm{FIAP}_X(n) = \frac{a_X^{\mathrm{sol}}(n,n) V_{\mathrm{leachate}}(n) + \sum_{i=1}^{n-1} a_X^{\mathrm{sol}}(i,n) V_{\mathrm{sample}}(i)}{A_X^{\mathrm{inv}}(n) f_{\mathrm{U}} m_{\mathrm{UO_2}}} \quad (2)$$

2.2.5. Solid characterization

A Jobin–Yvon LabRam Raman spectrometer was used in conjunction with a nuclearized microscope (Optique Peter, Lyon, France) with an objective turret (1.25×, 5×, 10×, 20×, 50× and 100×). A 532 nm YAG laser with output power adjustable from 20 to 120 mW was used with a variable filter to provide low excitation beam power levels. The optical microscope is mounted in a hot cell, while the Raman spectrometer and laser are installed outside the cell with a fiber-optic signal transmission line.

This optical spectroscopy technique has several advantages, including the following:

- No sample preparation was necessary, simplifying hot cell work and allowing direct observation of the formation of secondary phases on the spent fuel after leaching.
- Coupling with a nuclearized microscope provided a local probe (approx. 1 μm^3) that was ideal for investigating precipitates, thin oxidized layers, MOX aggregates, etc.).
- It was relatively easy to compare the spectra obtained with a library of characteristic spectra available in the literature or based on the synthesis of reference phases.

3. Results and discussion

3.1. Solution chemistry

3.1.1. Actinide chemistry

3.1.1.1. Actinide concentrations and redox potential of the bulk solution. Fig. 2 shows the uranium and plutonium concentrations versus time for experiments 1 and 2. In experiment 1 (benchmark experiment without external gamma irradiation) the uranium and plutonium concentrations clearly increased over time and steady-state conditions were not reached after two weeks of leaching in the bulk solution. The concentrations ranged from 10^{-8} mol L^{-1} to 3×10^{-7} mol L^{-1} for uranium and from 10^{-10} mol L^{-1} to 5×10^{-10} mol L^{-1} for plutonium. Leachate acidification and allowance for the acid rinses also showed increasing concentrations at the end of the test: 5×10^{-7} mol L^{-1} for uranium and 5×10^{-9} mol L^{-1} for plutonium.

Conversely, steady-state conditions were quickly reached in experiment 2. The uranium concentration at saturation was about 6×10^{-7} mol L^{-1} during the test and the total concentration increased to 3×10^{-6} mol L^{-1} after acidification of the experimental device and leachate. The plutonium concentration at saturation was about 6×10^{-8} mol L^{-1} and was practically unchanged after acidification. Compared with experiment 1, a significant increase in the actinide (uranium and plutonium) concentrations was observed in the presence of an external gamma irradiation source.

It is important to compare the concentration variations with the measured redox potential in the bulk solution (Fig. 3). The available data for MOX47 fuel show that the potential significantly increased during the initial instants of external gamma irradiation

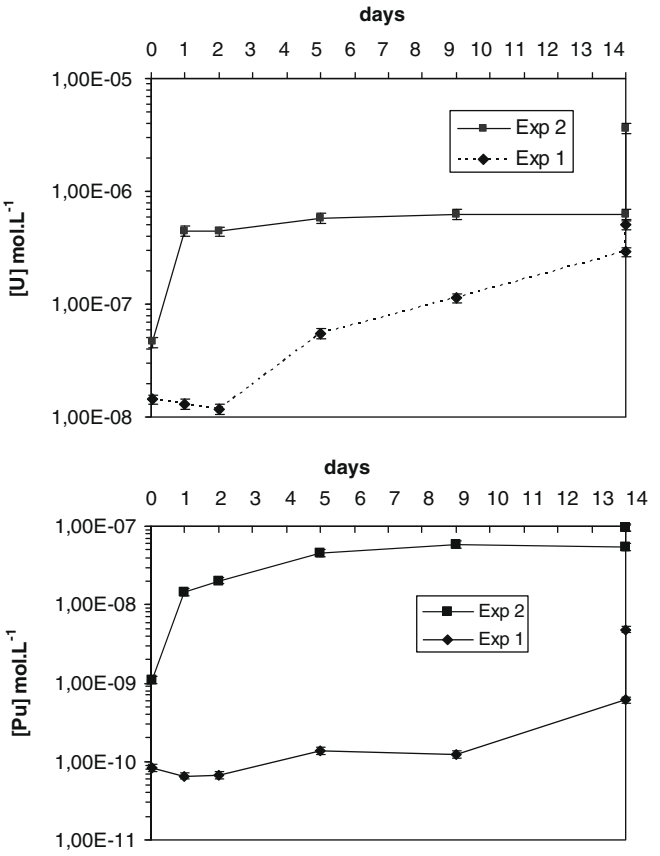

Fig. 2. Uranium and plutonium concentrations versus time for experiments 1 and 2.

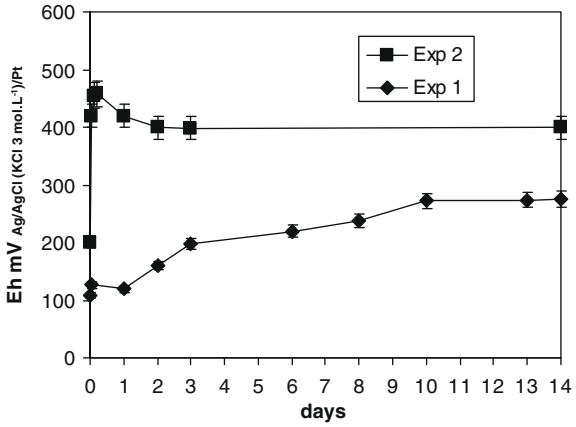

Fig. 3. Redox potential (Ag/AgCl electrode (KCl 3 mol L^{-1}) with platinum probe) of homogeneous solution versus time for experiments 1 and 2.

(experiment 2) followed by stabilization at about +400 mV (Ag/AgCl). With no external irradiation source (experiment 1) the measured potential was lower and continued to rise over time to about +280 mV (Ag/AgCl) (Fig. 3). No significant difference or variation was observed for the pH. After two weeks of leaching the pH was 6.9 for experiment 1 and 6.5 for experiment 2, compared with 6.2 at the beginning of the tests. These potential and pH values can account for the differences between the two experiments regarding the uranium and plutonium concentrations and solubility in the bulk solution.

Many published reports [14–19] are available for plutonium concerning thermodynamic data and the nature of the phases liable to control plutonium solubility as a function of the bulk solution pH and redox potential. The plutonium solubility obtained in experiment 2 – about 6×10^{-8} mol L^{-1} for a stable potential of +400 mV (Ag/AgCl) – reflects a major change in plutonium speciation under these experimental conditions due to high oxidation (mainly oxidation state V) [18] (Table 2). The Pourbaix diagram for plutonium in aqueous media (Fig. 4) also provides pertinent information and confirms that in the presence of an external gamma irradiation source the potential is high enough to oxidize plutonium to oxidation state V. In the absence of actual speciation of leachates for spent MOX47 fuel it is important to note that no plutonium colloids were detected at the end of experiment 2 (Fig. 5). This also corroborates the presence of plutonium at oxidation state V, as actinide colloids tend to form in the same order as they are hydrolyzed: $M^{+4} > MO_2^{2+} > M^{3+} > MO_2^{+}$ [19]. Conversely, in experiment 1 plutonium was found mainly at oxidation state IV based on the speciation diagram (Fig. 4).

The phases liable to control plutonium solubility (hydroxide, oxide, etc.) depending on the oxidizing conditions under radiolysis in contact with water have been a focus of discussion in the literature in recent years [14–22]. The experimental results presented here appear to be compatible with a conventional explanation based on an equilibrium with a $Pu(OH)_4$ phase. As indicated in Table 2, based on work by Haschke [18], the solubility limit of this phase appears to have been reached in experiment 2 (6×10^{-8} mol L^{-1}) at a potential of +400 mV (Ag/AgCl). As PuO_2^+ is the major species, enough plutonium must be dissolved to maintain the equilibrium with $Pu(OH)_4$, hence the increase in the total plutonium concentration. In experiment 1, however, the solubility limit of $Pu(OH)_4$ (about 2×10^{-9} mol L^{-1} [18]) was not reached at +280 mV (Ag/AgCl) after 2 weeks of leaching since the measured concentration in the bulk solution did not exceed 5×10^{-10} mol L^{-1}. However, can we discount the precipitation of plutonium hydroxide during experiment 1? Not if we allow for the uncertainties on the plutonium hydroxide solubility values reported in the literature, resulting in more than an order of magnitude of difference [14,15,18]. We may note in particular that at the beginning of experiment 1 the Pu concentration was stable at about 1×10^{-10} mol L^{-1}, as was the potential at +120 mV (Ag/AgCl). This concentration is compatible with solubility controlled by $Pu(OH)_{4(am)}$ [14,15,18]; the equilibrium then shifted slightly as the potential gradually increased to +280 mV (Ag/AgCl). Moreover, as discussed below, the release of fission products (alteration tracers) was considerably higher than for plutonium in experiment 1, implying that plutonium remained mainly (more than 90%) on the fuel surface.

The major uranium species in the neutral medium at the measured potentials was $UO_2(OH)_{2aq}$ [14,19] with uranium at oxidation state VI in both experiments. For experiment 1 the redox potential increase under water radiolysis due to the MOX47 fuel $\alpha\beta\gamma$ self-irradiation field could account for the persistence of oxidizing dissolution and the continuous uranium release. The uranium concentrations during this experiment were too low (3×10^{-7} mol L^{-1}) to observe any precipitation of schoepite $UO_2(OH)_2$ [14,19] from the bulk solution after 2 weeks of leaching. For experiment 2 the uranium concentrations and the hydrogen peroxide concentrations (6×10^{-5} mol L^{-1}) were compatible with the precipitation of uranium peroxide (studtite: $UO_4{\cdot}4H_2O$) [9,10] as discussed below. The more oxidizing conditions and greater material flows of this experiment allowed saturation with respect to this phase to occur quickly. It is also important to note that, unlike plutonium, most of the uranium was found in solution in colloid form, indicating that plutonium (Pu(V)) and uranium (U(VI)) exhibit distinctly different behavior in solution under external gamma irradiation.

3.1.1.2. Cumulative uranium and plutonium release fractions. The cumulative release fractions for experiments 1 and 2 are plotted versus time in Fig. 6.

MOX47 fuel is heterogeneous, and is characterized by the presence of plutonium-enriched aggregates. It is therefore interesting to observe and compare the behavior of plutonium and uranium in solution. Assuming preferential alteration of the basic UO_2

Table 2
Dependence of the plutonium concentration and oxidation state on the redox potential of the solution at equilibrium with $Pu(OH)_4$ (neutral water). Calculations by Haschke, 2002 [18].

Eh (mV/SHE)	Eh (mV) (Ag/AgCl)	[Pu] mol L^{-1}	log [Pu]	Pu(IV) (%)	Pu(V) (%)	Pu(VI) (%)
100	−107	1.74×10^{-9}	−8.76	99.99	0	0
200	−7	1.74×10^{-9}	−8.76	99.99	0	0
300	93	1.74×10^{-9}	−8.76	99.99	0.01	0
400	193	1.75×10^{-9}	−8.76	99.48	0.52	0
500	293	2.19×10^{-9}	−8.66	79.44	20.45	0
600	393	2.37×10^{-8}	−7.63	7.36	92.63	0
700	493	1.08×10^{-6}	−5.97	0.16	99.76	0.08
800	593	5.49×10^{-5}	−4.26	0	96.09	3.91

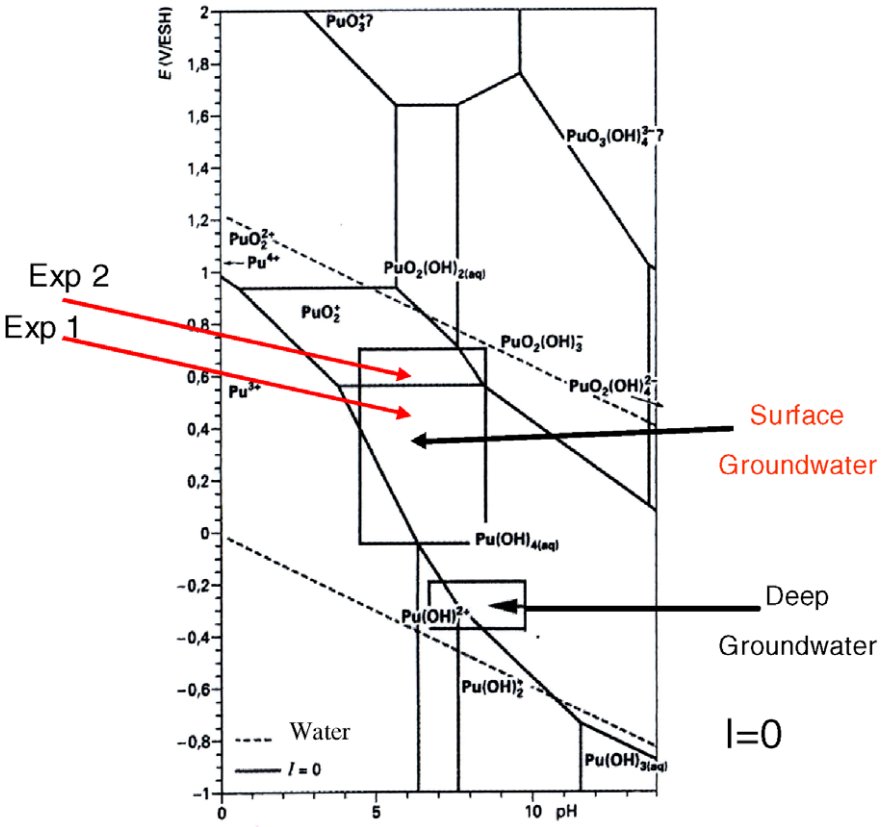

Fig. 4. Plutonium speciation diagram in noncomplexing aqueous medium (zero ionic strength) [16].

matrix compared with the plutonium-enriched aggregates or the intermediate phase, comparing the cumulative plutonium and uranium release fractions should reveal significant differences. This point must be considered in perspective, however, without overlooking the fact that redox potential gradients exist both on the fuel surface and between the aggregates and the UO_2 matrix, as well as between the surface and the bulk solution – especially in experiment 1.

For experiment 1 (Fig. 6), after acidification of the leachate and taking into account the acid rinses of the leaching device components, the uranium release is clearly greater than for plutonium (by about a factor of 4). This could be attributed to the combined effects of two phenomena:

- After oxidation at the aggregate/water interface, under high local $\alpha\beta\gamma$ dose rates plutonium precipitates in particular on the fuel surface. Without a gamma irradiation source, plutonium release is limited in the bulk solution and it tends to reprecipitate on the surface of the UO_2 matrix. This phenomenon was probably less evident for uranium, which remained at oxidation state VI.
- The plutonium-enriched aggregates and possibly the intermediate phase are more stable than the UO_2 matrix altered mainly by water radiolysis and by the MOX47 $\alpha\beta\gamma$ self-irradiation field, ultimately resulting in major differences between the uranium and plutonium release.

For experiment 2 (Fig. 6), unlike experiment 1, the cumulative uranium and plutonium release fractions after acidification were near 1 (FIAP(Pu)/FIAP(U) = 0.8 to 0.9). The very oxidizing conditions in the bulk solution (forming Pu(V)) revealed by the redox potential measurement (+400 mV (Ag/AgCl)) suggest two hypotheses:

- The entire spent fuel matrix – the plutonium-enriched aggregates, the intermediate zone, and the UO_2 matrix – is destabilized. This destabilizing effect on the aggregates and the intermediate phase is accompanied by a significant increase in the plutonium solubility in the bulk solution and greater plutonium release in the presence of an external irradiation source (Fig. 2).
- The aggregates are not necessarily destabilized, but the more oxidizing conditions result in greater leaching of the other zones (UO_2 matrix or even the intermediate phase) together with greater release of the plutonium (found in appreciable quantities in these phases) toward the bulk solution.

These hypotheses are discussed below in greater detail with regard to surface characterization by Raman spectroscopy and a comparison of the oxidation of the aggregates and the matrix.

3.1.2. Hydrogen peroxide formed by radiolysis in the bulk solution

Fig. 7 shows the variation over time of the hydrogen peroxide concentrations in the bulk solution for experiments 1 and 2. The hydrogen peroxide concentration variation due to water radiolysis can be attributed to concentrations gradients of oxidizing species as already discussed by Jégou et al. [10] for spent UOX60 fuel.

With an external gamma irradiation source, all the bulk solution is irradiated at a high gamma dose rate and steady-state values are quickly reached for the redox potential and hydrogen peroxide concentration. The fact that after only a few instants the hydrogen peroxide concentration stabilized at 6×10^{-5} mol L^{-1} in the bulk solution during experiment 2 corroborates this observation. Moreover the external gamma irradiation contributes to maintain a high

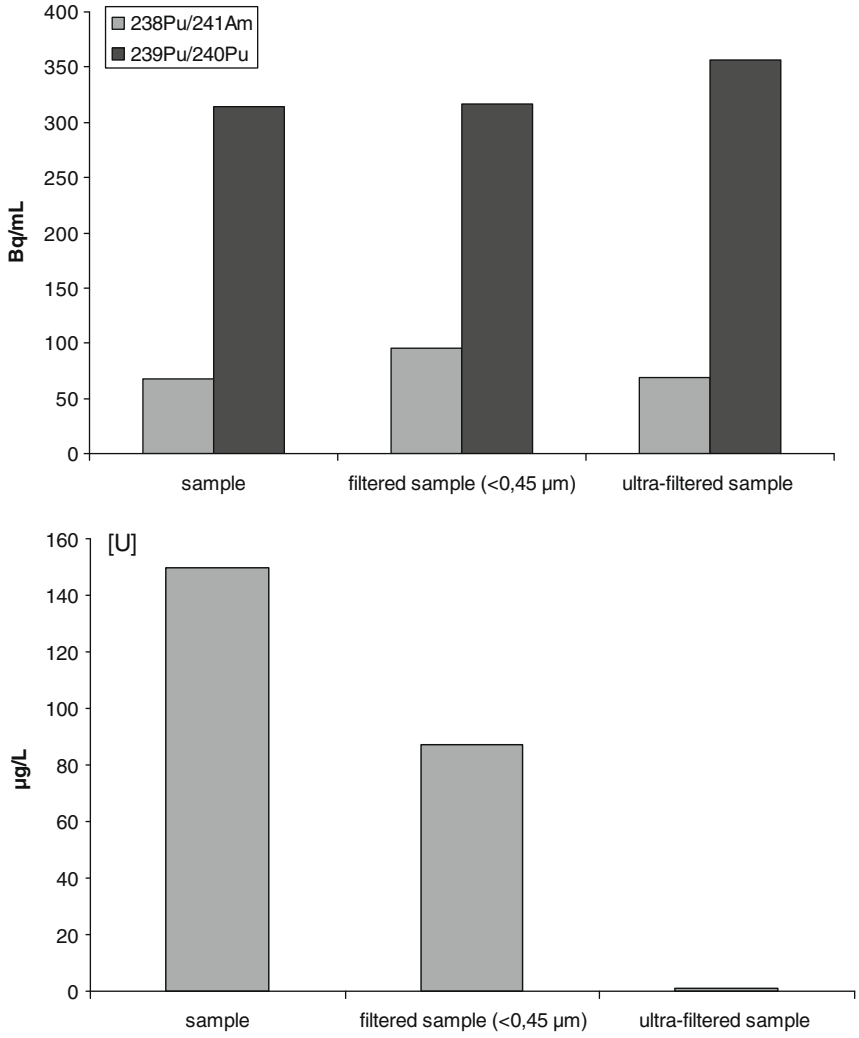

Fig. 5. Plutonium and uranium activities or concentrations in homogeneous solution after filtration (0.45 μm) and ultrafiltration (10,000 Da) at the end of the experiment 2.

concentration of hydrogen peroxide at the solid/liquid interface and limits the diffusion from the interface to the bulk.

Without the source, αβ irradiation was highly localized on the MOX47 fuel surface and considering the fuel masses involved, γ irradiation of the bulk solution was limited[1]. Hydrogen peroxide is produced mainly at the interface and diffuses into the bulk solution. The hydrogen peroxide concentrations in the bulk solution were thus lower for experiment 1, not exceeding 1×10^{-6} mol L^{-1} (Fig. 7).

The differences in the hydrogen peroxide concentrations for experiments 1 and 2 are also consistent with the measured redox potentials since the conditions were less oxidizing for experiment 1 than for experiment 2, although the concentration rose to a peak in experiment 1 but not in experiment 2. A realistic hypothesis would be that a fraction of the hydrogen peroxide produced was consumed by the formation of secondary phases and oxidation reactions. This consumption could have competed with the formation and diffusion of H_2O_2 into the homogeneous phase in experiment 1, but this was not the case for experiment 2 as the consumption was masked by the strong external gamma irradiation of the bulk solution.

[1] The gamma dose rate in the bulk solution was estimated using microshield® at about one gray per hour.

3.1.3. Fission product behavior

It is difficult to reach conclusions concerning fuel alteration based on the actinide chemistry in the bulk solution because of the high redox potential gradients in the system and the absence of complexing agents. The fission products, after elimination of the instant release inventories, remain the best alteration tracers under these experimental conditions.

Only the cesium and strontium release fractions are presented and discussed here. The fact that the Cs/Sr congruence ratios are near 1 (Fig. 8) for both experiments 1 and 2 indicates that this parameter describes the dissolution of the MOX47 fuel "matrix" in the general sense – i.e. the UO_2 matrix or the Pu-enriched aggregates – under different oxidizing conditions.

The fission product release fractions are significantly greater (by about an order of magnitude) than for the actinides in both experiments, suggesting that most of the actinides are retained on the fuel surface and confirming that it is difficult to draw conclusions about matrix alteration based on the behavior of the actinides in solution alone.

The $^{134/137}$Cs and ^{90}Sr release fractions with an external irradiation source (experiment 2) were 2 to 3 times greater than in the benchmark experiment. MOX47 fuel is therefore leached to a greater extent under external irradiation. A significant difference can be observed between experiments 1 and 2 when the release fractions are plotted versus time (Fig. 8). For experiment 2, with

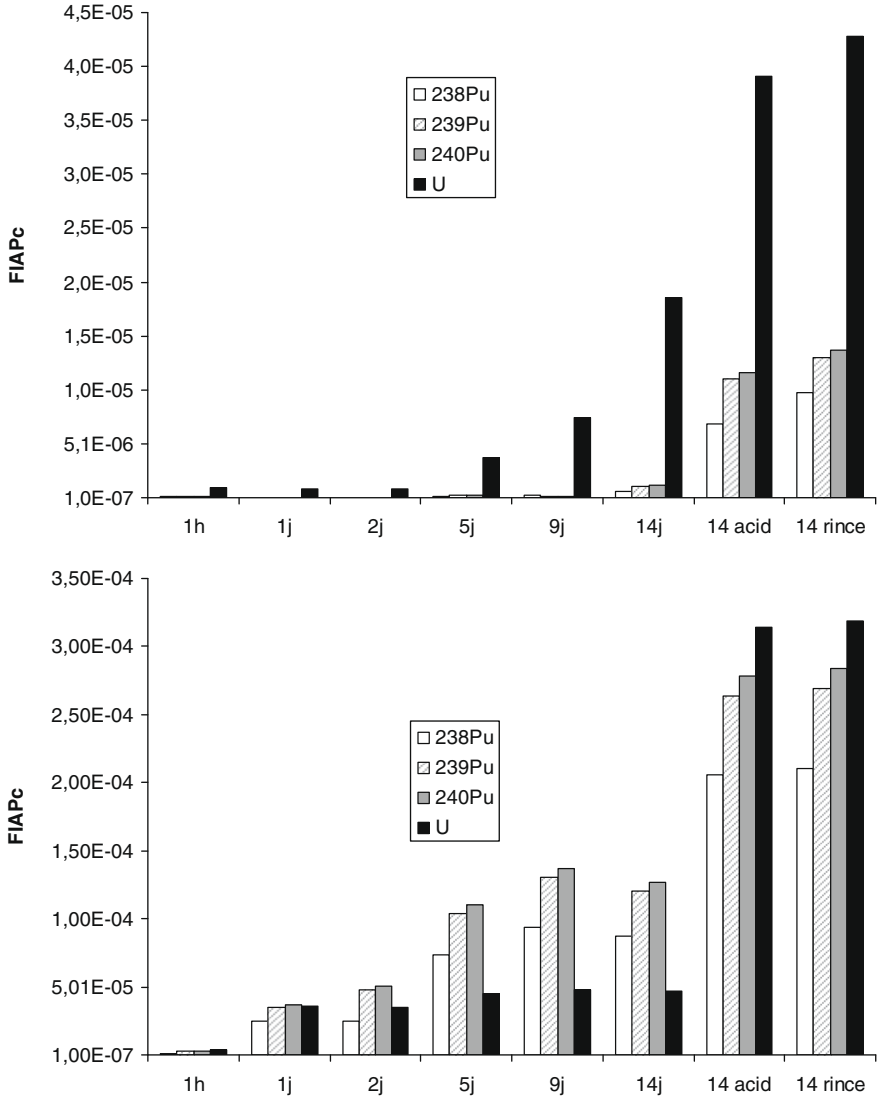

Fig. 6. Cumulative uranium and plutonium release fractions versus time for experiments 1 (top) and 2 (bottom).

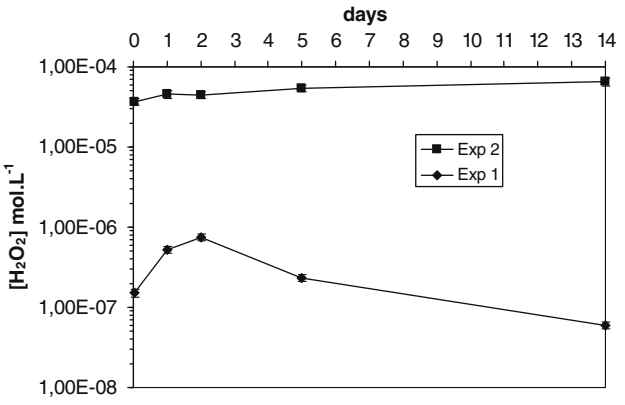

Fig. 7. Hydrogen peroxide concentrations versus time for experiments 1 and 2.

an external gamma irradiation source, the dissolution rate diminishes over time. Fitting the releases to $\sqrt{t}$ gives a linear progression with a correlation coefficient of 0.996 corresponding to diffusive control of alteration, whereas for experiment 1 a linear fission product release is observed over time. Slight strontium sorption is observed over time, but disappears when acidification is taken into account at the end of the experiment (return to linearity). Linear conditions imply that the actinide concentrations did not stabilize in the bulk solution, contrary to experiment 2.

3.2. MOX47 fuel surface characterization by Raman spectroscopy

3.2.1. General

Raman spectroscopy characterization was performed primarily to compare the oxidation of the plutonium-enriched aggregates with that of the UO_2 matrix when subjected to radiolytic oxidation. Both regions are easily discriminated by optical microscopy, whereas this is more difficult for the intermediate phase over time. Can the high plutonium concentrations in the aggregates limit fuel oxidation locally? How does the surface react to oxidation depending on the intensity of the oxidizing conditions? This information should also support the hypotheses postulated on the basis of solution chemistry data for experiments 1 and 2. The second objective of characterization is to identify possible secondary phases precipitated on the MOX47 fuel surface.

The characterization sample was an irradiated MOX47 fuel segment that was polished and then leached for 3 months in pure aerated water in the presence of an external gamma irradiation

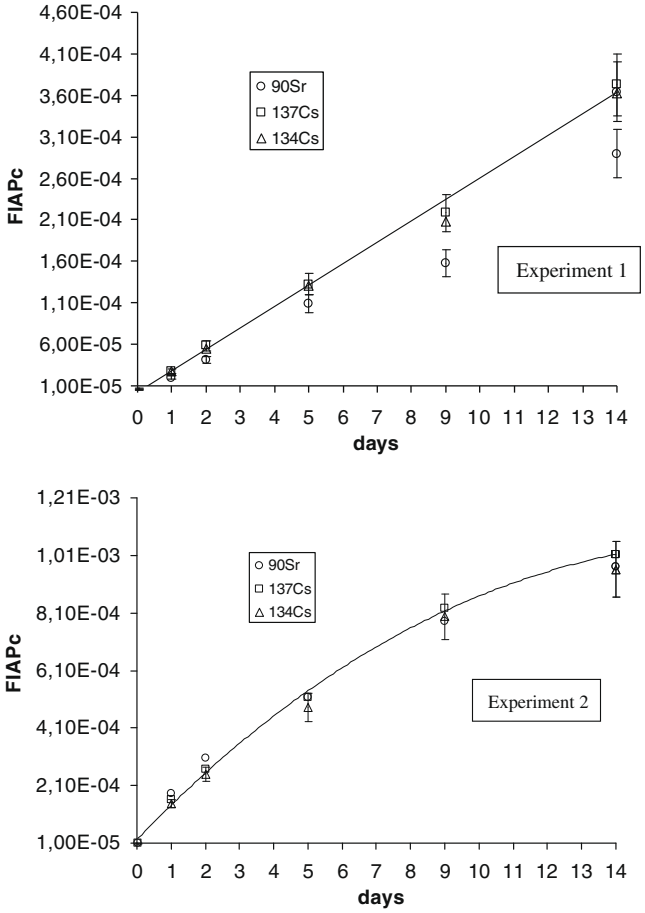

Fig. 8. Fission product release fractions ($^{134/137}$Cs et ^{90}Sr) versus time for experiments 1 and 2.

source. Spectra were acquired on the outermost surface after various time intervals. In order to obtain representative data concerning oxidation of the surface subjected to radiolytic oxidation, the spectrum acquisition parameters (laser power and acquisition time) were optimized on UO_2 benchmark samples, on UO_2 samples doped with 1 wt.% Pu, and on unirradiated and unleached PuO_2 samples [4]. The purpose of this optimization was to avoid any significant change (oxidation in particular) of the surface due to local heating by the laser beam. The laser was operated at minimum power and a 30% attenuation filter was inserted in the beam path. The power reaching the sample surface was about 1 to 2 mW [4].

Raman spectroscopy can provide important data on structural changes in the oxides and solid solutions as long as they result in changes to the crystal symmetry. Group theory can then be used to predict the Raman-active vibration modes likely to appear during oxidation. Recently published work on unirradiated UO_2 [23–28] showed that UO_2 oxidation results in significant changes in the crystal structure (UO_2 (cubic Fm-3m) → U_4O_9 (cubic I-43d) → U_3O_7 (tetragonal I4mmm) → U_3O_8 (orthorhombic C2 mm or hexagonal P-62 m)). Conversely, PuO_2 is much less subject to oxidization; this topic has been widely examined and discussed in recent years [20–22], and a recent explanation for this phenomenon is based on the relative positions of the 5f electrons with respect to the O2p band. Oxidation is easy if this band is situated below the 5f levels, as for UO_2; conversely, if the levels overlap oxidation is no longer possible (as in the case of PuO_2) [22]. Nevertheless, some doubt remains concerning the oxidation of plutonium under water radiolysis, as these energy levels can be reversed. Calculations [21] have shown that PuO_2 oxidation by H_2O_2 could be favored from an energy standpoint, with the formation of Pu_4O_9 as an intermediate reaction product on the oxide surface. In our experiments with an external gamma irradiation source all these conditions occur (highly oxidizing conditions and the presence of water) and it is essential to determine the site of the plutonium oxidation reaction: does it occur only in solution in contact with H_2O_2 [29], or rather on the oxide surface? The alteration of the plutonium-enriched aggregates also depends to a large extent on these processes because without oxidation of plutonium on the surface, uranium oxidation could be the limiting step in dissolution of aggregates, with the formation of Pu(V) occurring subsequently in the bulk solution.

To the best of our knowledge no Raman spectroscopy data are available in the literature concerning the oxidation behavior of spent MOX fuel.

3.2.2. Characterization of a MOX47 fuel segment leached for 3 months under external gamma irradiation

3.2.2.1. Initial characterization prior to leaching. Fig. 9 shows an optical micrograph of the MOX47 fuel surface before and after chemical etching to reveal the aggregates. This step was indispensable to allow subsequent comparisons of the Raman spectra for each zone over time.

Fig. 10 shows the initial Raman spectra of the UO_2 grains of the spent MOX47 fuel and the plutonium-enriched aggregates. The Raman spectrum of a PuO_2 sample was also obtained for comparison. The sample came from a 30-year old PuO_2 source used such as a pacemaker battery [30], and was thus not irradiated. Conversely, because of its initial isotopic composition (90% ^{238}Pu) the sample was severely damaged (about 100 displacements per atom) and contained about 20% ^{234}U produced by alpha decay [31].

With regard to the MOX47 fuel, and more specifically the Raman spectrum of the UO_2 matrix surrounding the Pu aggregates, three peaks characteristic of UO_2 are clearly visible. UO_2 has a fluorite structure with an Fm-3m space group (O_h symmetry). Group theory predicts the existence of two vibration modes: $T_{2g} + T_{1u}$. The first threefold degenerate vibration mode is only Raman-active (447 cm^{-1} in Fig. 10) and the second only infrared-active [23,28]. The 580 cm^{-1} peak in Fig. 10 is generally attributed to UO_2 matrix defects [26] that affect the selection rules. The origin of the 1150 cm^{-1} peak remains a subject of discussion in the literature; it was initially attributed to the $\Gamma_5 \rightarrow \Gamma_3$ electronic transition [23], then more recently to a 2LO vibration band [32] (the first order LO phonon being the 580 cm^{-1} peak). It is important to note that the irradiated UO_2 matrix of MOX47 fuel exhibits a classic spectrum relatively unaffected by irradiation. Moreover, the very distinct peak at 1150 cm^{-1} characteristic of unoxidized or very slightly oxidized UO_2 samples [23] clearly demonstrates that chemical etching and water rinsing of the fuel sample surface did not significantly modify (oxidize) the material.

Before considering the spectra corresponding to the Pu aggregates it is interesting to examine the PuO_2 sample. The structure of PuO_2, identical to that of UO_2, is a fluorite with an O_h space group (Fm-3m); both vibration modes $T_{2g} + T_{1u}$ are therefore present and only the first is Raman-active. The T_{2g} mode is situated at 469 cm^{-1} in this case (Fig. 10). The 638 cm^{-1} peak is attributable to matrix defects [4], as in the case of UO_2. In sum, the only difference in the spectra of the UO_2 and PuO_2 matrices is a shift in the vibration bands.

The Raman spectra for the plutonium-enriched aggregates include two peaks at 454 and 580 cm^{-1} with a shoulder at 638 cm^{-1}; this portion of the spectrum can be attributed to the convolution of the UO_2 and PuO_2 source contributions. For the Pu aggregate in MOX47 fuel the 454 cm^{-1} peak can be interpreted using PeakFit® as the sum of two contributions (two Gaussian peaks): one at 447 cm^{-1} for uranium (49.1% of the signal) and

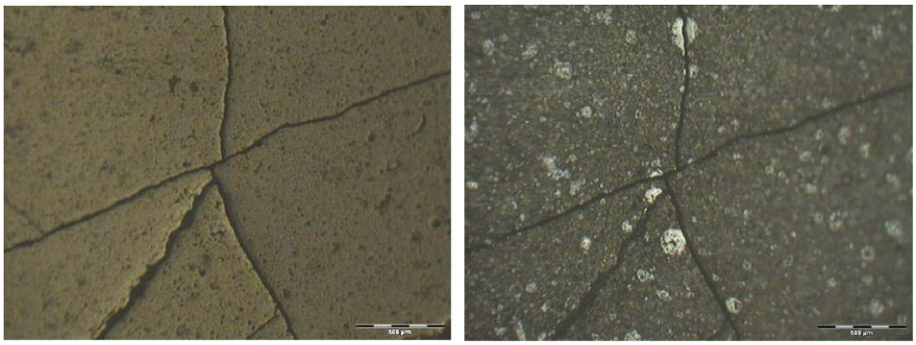

Fig. 9. Optical microscope observations of central zone of irradiated MOX47 sample before (a) and after (b) chemical etching.

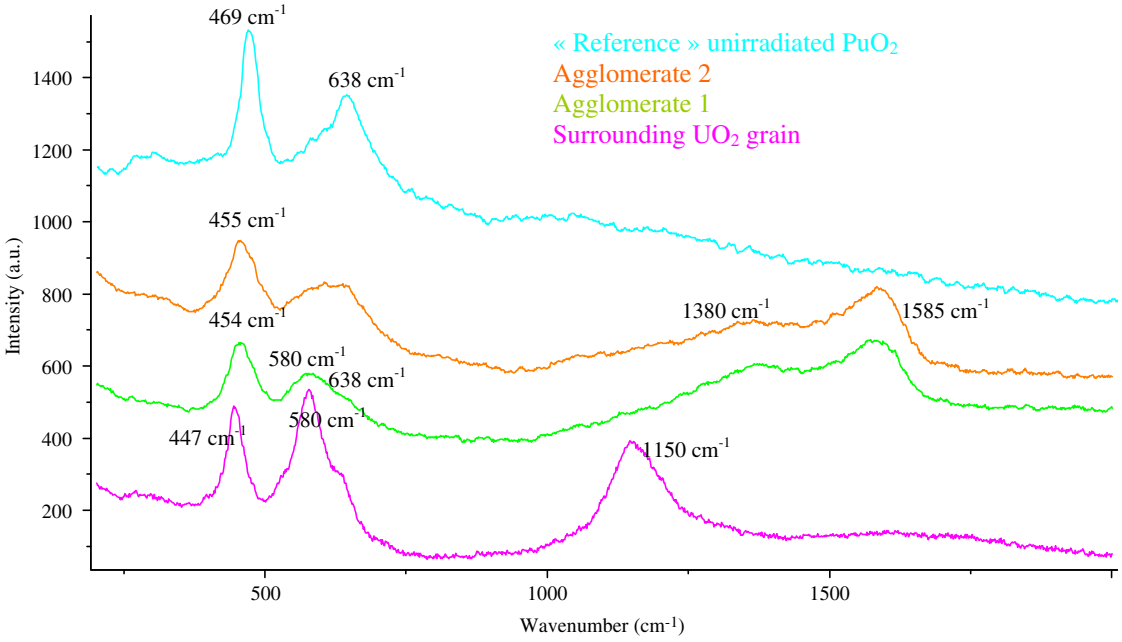

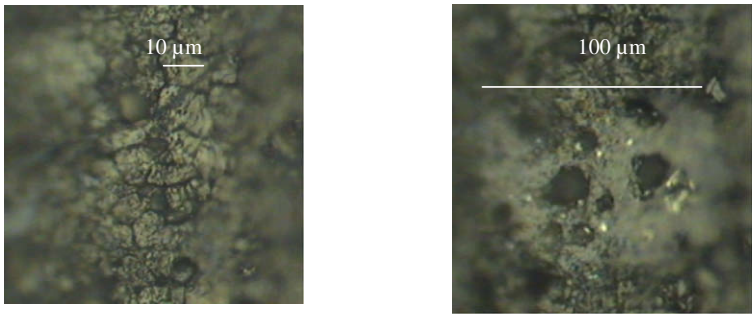

(a) Surrounding UO_2 grains (5-10 µm) (b) Agglomerate 1 (100 µm)

Fig. 10. Raman spectra and optical microscope images prior to leaching of plutonium-rich aggregates (arbitrarily designated 1 and 2) and surrounding UO_2 grains in MOX47 spent fuel. The Raman spectrum of an unirradiated PuO_2 sample was considered as a benchmark.

the other due to plutonium at 469 cm^{-1} (50.9% of the signal). The second peak at 580 cm^{-1} and the shoulder at 638 cm^{-1} were interpreted by PeakFit® as due mainly to uranium (about 65.6%) with 34.4% for the plutonium signal. In the region beyond 1000 cm^{-1} for the aggregate spectrum the 1150 cm^{-1} peak for UO_2 is not distinctly observed, and we are currently unable to account for the peaks at 1380 and 1585 cm^{-1}. This signal could be attributable to a Raman-active vibration mode or to a luminescence signal from another element. The Raman spectrometry characterization of unirradiated MOX fuel pellets will subsequently allow us to compare the Raman signal before and after irradiation and perhaps to determine the origin of this contribution.

3.2.2.2. Characterization during the leaching experiment under external gamma irradiation. The evolution of the Raman spectra and of the surface of a Pu aggregate over time are shown in Figs. 11a

and 11b. Except for the disappearance of the 1380 et 1585 cm^{-1} peaks after only 18 days of leaching there was generally little change in the spectra in terms of the appearance of new peaks indicative of changes in the crystal structure and oxidation of the aggregates as is the case for UO_2 [23,27,28]. The Pu-enriched aggregates appear to be relatively stable under radiolytic oxidation at 25 °C. These findings are consistent with recent work by Jégou et al. on actinide oxides [4], although the shape of the peaks differed from those recorded prior to leaching. The 580 cm^{-1} peak attributed to UO_2 was replaced by a peak at 638 cm^{-1} "characteristic" of PuO_2 and/or structural distortion into the fluorite structure. PeakFit® determined that the Pu component of the signal was 98% compared with 34.4% initially. Except for the 18-day spectrum in which the Pu signal component rose to 84% compared with 50.9% initially, this trend was less pronounced for the 454 cm^{-1} peak. Two hypotheses can be considered to account for this behavior: plutonium enrichment of the aggregates, or a change in the uranium signal in this wave number range due to slight uranium

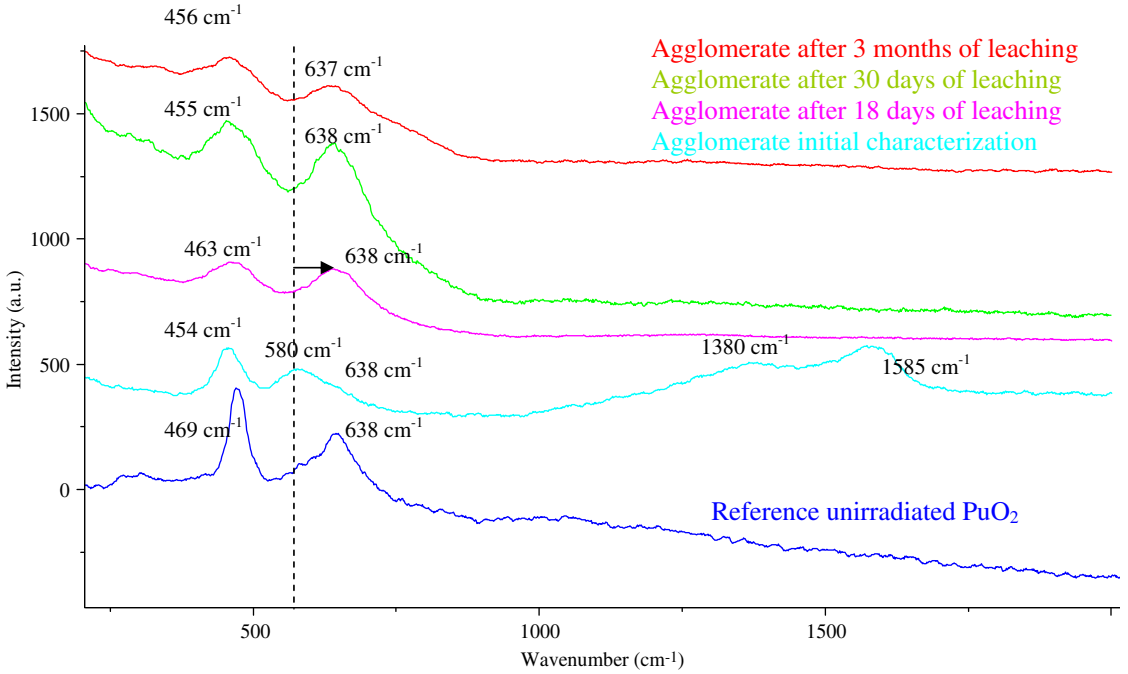

Fig. 11a. Raman spectra of a single plutonium-enriched aggregate during 3 months of leaching of a spent MOX47 fuel segment. The Raman spectrum of an unirradiated PuO_2 sample is shown for comparison.

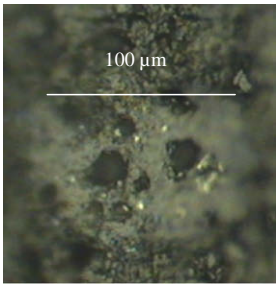

Agglomerate initial characterization

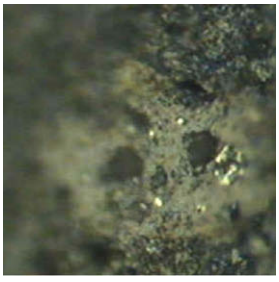

Agglomerate after 18 days of leaching

Agglomerate after 30 days of leaching

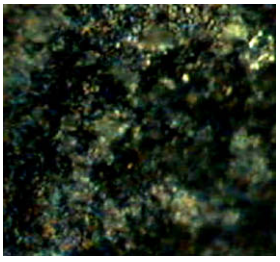

Agglomerate after 3 months of leaching

Fig. 11b. Optical microscope images of a single plutonium-enriched aggregate during 3 months of leaching of a spent MOX47 fuel segment.

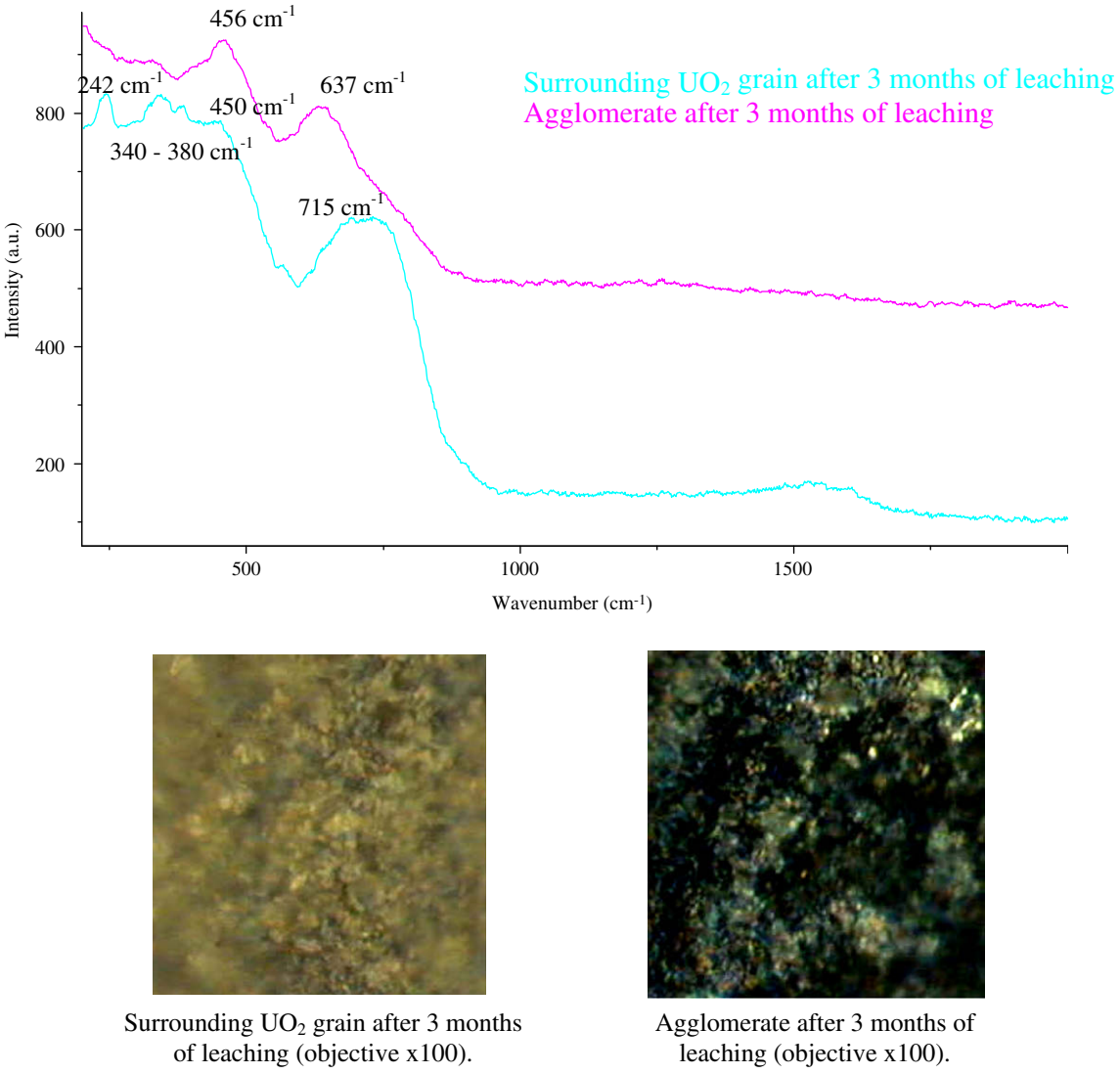

Fig. 12. Comparison of Raman spectra of the UO_2 matrix and a Pu aggregate (after 3 months of leaching) and corresponding optical microscope images.

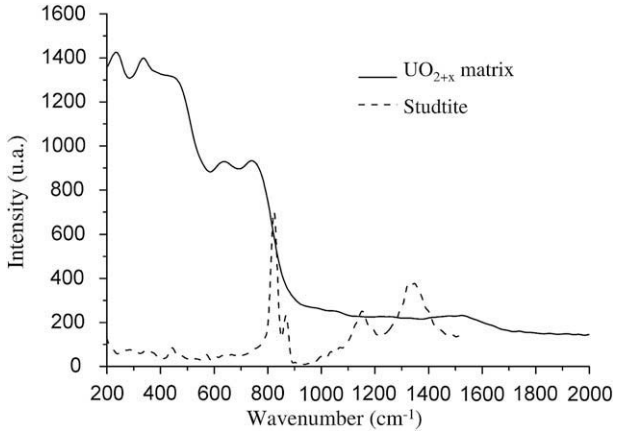

Fig. 13. Raman spectra of UO_2 grain surfaces after 3 months of leaching of a spent MOX47 fuel segment.

oxidation (structural distortions within the anion sublattice could be accompanied by an increase of the intensity of the 638 cm^{-1} peak).

To confirm the stability of the Pu aggregates it is interesting to compare the Raman spectrum of the encapsulating UO_2 matrix with that of the Pu aggregates after 3 months of leaching under external gamma irradiation (Fig. 12). The surface of the encapsulating UO_2 matrix appears yellowish due to the presence of small crystals after 3 months of leaching (Fig. 12); two types of Raman spectra (Fig. 13) were obtained depending on the laser beam focusing or the selected zone.

- The "surrounding UO_2 grain" spectrum in Fig. 12 was obtained for the MOX47 fuel UO_2 matrix after 3 months of leaching. The disappearance of the 1150 cm^{-1} peak compared with the spectrum obtained prior to leaching very clearly indicates uranium oxidation [23]. Significant changes in the spectrum of the encapsulating UO_2 matrix are also visible, with new peaks at 340, 380 and 715 cm^{-1} and a generally stronger signal between 410 and 480 cm^{-1} (Fig. 12). These findings point to major oxidation of the UO_2 matrix under radiolysis compared with the Pu aggregates (Fig. 12). It is difficult to quantify the change in the O/U ratio for the UO_2 matrix of MOX47 fuel. However, UO_2 oxidation – which involves changes in the crystal structures resulting in new Raman-active peaks and significant spectrum modifications – has been investigated on unirradiated materials

[23–25,27,28]. The formation of orthorhombic U_3O_8 results in the appearance of A_{1g} and E_g vibration modes at wave numbers of about 340–350–410 cm^{-1} (A_{1g} U—O stretching vibration), 480 cm^{-1} (E_g U—O stretching vibration) and 750 cm^{-1} (combination of two A_{1g} U—O stretching bands). These are comparable to the values obtained for the MOX47 fuel UO_2 matrix after radiolytic oxidation, indicating appreciable oxidation of the UO_2 grains compared with the Pu aggregates under external irradiation. This result corroborates the hypothesis that the release of actinides and fission products in solution under external gamma irradiation is not attributable to destabilization of the Pu aggregates even under these highly oxidizing conditions, but rather to a larger contribution from the zones of lower plutonium enrichment that contain some 60% of the total plutonium.

- The "studtite" spectrum in Fig. 13 was obtained for the outermost surface and in the areas of high yellowish crystal density. This spectrum shows two peaks at 821 (U═O stretching) and 867 cm^{-1} (O—O stretching) that are characteristic of uranium peroxide, i.e. studtite with the formula $UO_4{\cdot}4H_2O$ [33,34]. The formation of this compound is not surprising considering the concentrations of hydrogen peroxide (6×10^{-5} mol L^{-1}) and uranium in the bulk solution. Beneath this studtite layer the spectrum was systematically characteristic of a highly oxidized compound (Fig. 13) indicating that secondary phases precipitated on the surface of the oxidized layer.

4. Conclusions

The mechanisms of oxidizing dissolution of spent MOX fuel (MIMAS TU2®) subjected to water radiolysis were investigated experimentally by leaching spent MOX47 fuel samples in pure water at 25 °C under different oxidizing conditions. The leached surfaces were characterized by Raman spectroscopy, which is now available for use in a hot cell environment with its uniquely powerful capability for analyzing the leached surfaces of these very heterogeneous irradiated materials at the scale of a cubic micrometer.

This study has shown that the heterogeneity of MOX47 fuel makes it difficult to interpret leach tests results based on bulk solution analysis. Nevertheless, this work has demonstrated that the highly oxidizing conditions induced by an external gamma irradiation source result in a significant increase in the solubility of plutonium (Pu(V)) and uranium (U(VI)) compared with a benchmark experiment performed without external irradiation. $(U_{1-y}Pu_y)O_2$ matrix oxidation is highly dependent on the Pu concentration, making it difficult to accurately determine whether the actinides come from the UO_2 matrix, the intermediate zone, or the Pu aggregates in MOX47 fuel. However, Raman spectroscopy demonstrated that the surrounding UO_2 matrix was much more sensitive to oxidation than the Pu aggregates, which appear to be more stable over time; this does not argue in favor of a significant contribution from the aggregates to the releases in solution. In particular, the Pu aggregates show no significant spectral evolution in terms of the appearance of new peaks that could indicate major changes in the crystal structure and extensive oxidation of the aggregates as is the case for UO_2.

The fission product release – considered as a general indicator of matrix alteration – from MOX47 fuel also increases under external gamma irradiation and a change in the leaching mode is observed. Diffusive conditions were clearly identified coinciding with the rapid onset of steady-state actinide concentrations in the in the bulk solution. With regard to the precipitation of secondary phases, only studtite has been identified to date on the surface of the UO_2 grains and no precipitate has been identified on the surface of the Pu aggregates. This implies that it is unnecessary to take into account any more detrimental degradation mechanism for MOX fuel than for UOX fuel in an incident scenario corresponding to a cladding failure.

Future experiments on homogeneous $(U_{1-y}Pu_y)O_2$ solid solutions will allow us to determine the influence of plutonium on MOX fuel oxidation under radiolysis. The site of the plutonium oxidation reaction must also be determined: does it occur only in solution in contact with H_2O_2 formed by radiolysis, or rather on the oxide surface? Although the hypothesis that plutonium solubility is controlled by $Pu(OH)_4$ found mainly on the fuel surface pleads in favor of plutonium oxidation in the bulk solution, it will be important in the future to assess the uranium behavior according to the plutonium concentration: could uranium oxidation eventually lead to dissolution of the aggregates?

Characterization of spent MOX47 fuel by Raman spectroscopy will continue on samples leached for extended time periods with and without an external gamma irradiation source. Additional isotopes (^{18}O, etc.) will also be added to the solutions to examine the oxidizing dissolution mechanisms.

Acknowledgements

This study was carried out under the PRECCI research program funded jointly by the CEA and EDF. The authors are grateful to the DHA colleagues and to the personnel of Atalante for their technical support.

References

[1] R.S. Forsyth, L.O. Werme, J. Nucl. Mater. 190 (1992) 3–19.
[2] R.S. Forsyth, The SKB spent fuel corrosion program, SKB Technical Report 97-25, December 1997.
[3] C. Jégou et al., J. Nucl. Mater. 326 (2004) 144–155.
[4] C. Jégou et al., J. Nucl. Mater., submitted for publication.
[5] A. Bouloré, Étude et modélisation de la densification en pile des oxydes nucléaires UO2 et MOX. Ph.D. Thesis, Institut National Polytechnique de Grenoble et École Nationale Supérieure des Mines de Saint-Étienne N 249 TD, France, 2001.
[6] C. Sari, J. Nucl. Mater. 35 (1970) 267–277.
[7] T.L. Markin, R.S. Street, J. Inorg. Nucl. Chem. 29 (9) (1967) 2265–2280.
[8] J.P. Grouiller, J. Pavageau, In synthesis on the spent nuclear fuel evolution, CEA R-5958 Report (ISSN0429-3460), 2001, 616p.
[9] C. Jégou et al., J. Nucl. Mater. 341 (2005) 62–82.
[10] C. Jégou et al., Radiochim. Acta 95 (2007) 513–522.
[11] T. Lundström, Ph.D. Thesis, Linköpings Universitet, Sweden, 2003.
[12] A. Poulesquen, C. Jégou, J. Nucl. Technol. 160 (3) (2007) 337–345.
[13] H. Christensen, S. Sunder, J. Nucl. Mater. 238 (1996) 70–77.
[14] P. Vitorge et al., J. Nucl. Sci. Technol. (Suppl. 3) (2002) 713–716.
[15] V. Neck et al., J. Alloys Compd. 444–445 (2007) 464–469.
[16] V. Neck et al., Radiochim. Acta 95 (2007) 193–207.
[17] J.M. Haschke, V.M. Oversby, J. Nucl. Mater. 305 (2002) 187–201.
[18] J.M. Haschke, R.L. Bassett, Radiochim. Acta 90 (2002) 505–509.
[19] P. Toulhoat et al., Migration ou confinement des radioéléments? L'actualité chimique. Avril-Mai 2005-N 285-286, Ed. Société Française de Chimie, pp. 41–53.
[20] J.M. Haschke et al., Science 287 (2000) 285.
[21] P.A. Korzhavyi et al., Nature Mater. 3 (2004) 225–228.
[22] D.A. Andersson et al., Phys. Rev. B 79 (2009) 024110-1.
[23] D. Manara, B. Renker, J. Nucl. Mater. 321 (2003) 233–237.
[24] S.D. Senanayake, H. Idriss, Surf. Sci. 563 (2004) 135.
[25] S.D. Senanayake et al., J. Nucl. Mater. 342 (2005) 179–187.
[26] P.R. Graves, Appl. Spectrosc. 44 (1990) 1665–1667.
[27] G.C. Allen et al., J. Nucl. Mater. 144 (1987) 17–19.
[28] M. Luisa Palacios, S.H. Taylor, Appl. Spectrosc. 54 (2000) 1372–1377.
[29] V.P. Shilov et al., Radiochemistry 38 (1996) 217–219.
[30] R. Boucher, Y. Quere, J. Nucl. Mater. 100 (1981) 132–136.
[31] D. Roudil et al., in: Scientific Basis for Nuclear Waste Management XXIX Mat. Res. Soc. Symp. Proc., vol. 932, Ghent, 2005, pp. 529–536.
[32] T. Livneh, E. Sterer, Phys. Rev. B 73 (2006) 085118-1.
[33] S. Bastians et al., J. Raman. Spectrosc. 35 (2004) 726.
[34] M. Amme et al., J. Nucl. Mater. 306 (2002) 202–212.